

Cross-Shape Graph Convolutional Networks

Dmitry Petrov, Evangelos Kalogerakis

University of Massachusetts, Amherst

Abstract. We present a method that processes 3D point clouds by performing graph convolution operations across shapes. In this manner, point descriptors are learned by allowing interaction and propagation of feature representations within a shape collection. To enable this form of non-local, cross-shape graph convolution, our method learns a pairwise point attention mechanism indicating the degree of interaction between points on different shapes. Our method also learns to create a graph over shapes of an input collection whose edges connect shapes deemed as useful for performing cross-shape convolution. The edges are also equipped with learned weights indicating the compatibility of each shape pair for cross-shape convolution. Our experiments demonstrate that this interaction and propagation of point representations across shapes makes them more discriminative. In particular, our results show significantly improved performance for 3D point cloud semantic segmentation compared to conventional approaches, especially in cases with limited number of training examples.

Keywords: geometric deep learning, 3D point clouds, shape segmentation, cross-shape convolution, cross-attention.

1 Introduction

Learning geometric representations is fundamental to shape understanding and processing. Over the recent years, there has been significant research in developing deep networks that operate directly on 3D point clouds. Inspired by advances of deep learning on graphs, several architectures have been proposed to learn point-wise representations of shapes through graph convolution and attention layers [1,2,3,4,5,6,7]. The layers of these networks output a representation for each point by weighting and aggregating representations and relations with other points within the same input point set. In this manner, these networks hierarchically encode shape structure useful for performing high-level tasks, such as shape segmentation.

In this paper, we propose to extend graph convolution and attention to operate *across shapes of an input collection* (Figure 1). In our architecture, the representation of a point in a shape is learned by combining representations originating from points in the same shape as well as other shapes. The rationale for such approach is that if a point on one shape is related to a point on another shape e.g., they lie on geometrically or semantically similar patches or parts,

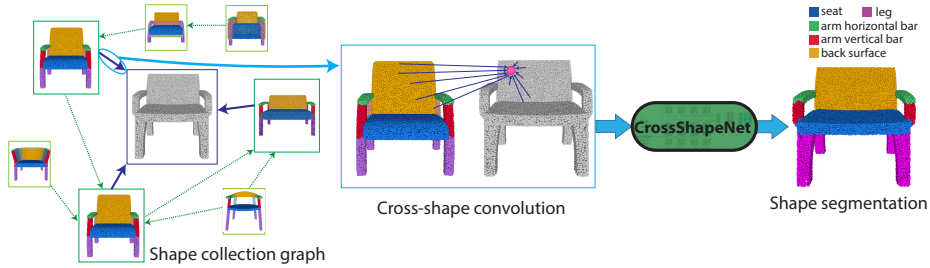


Fig. 1: (Left) Given an input training collection of shapes, our method builds a shape collection graph whose nodes represent shapes (in green box) and edges represent selected pairs for training our cross-shape convolution layers. At test time, given a new shape (in blue box), relevant training shapes are selected as its neighborhood. (Middle) Our trained network executes cross-shape convolutions to propagate point representations from training shapes to the test shape. The test point representations are computed by combining point representations from other shapes, weighted by an attention mechanism. Thicker arrows indicate higher attention, which tends to correlate points within geometrically and semantically similar parts. (Right) Our network is demonstrated for shape segmentation on PartNet. (Note:) In the collection graph (left), and cross-shape convolution example (middle), a subset of edges is shown for didactic reasons.

then cross-shape convolution can promote consistency in their resulting representations and part label assignments. Our approach is also inspired by early shape segmentation approaches that transfer deformable part templates across shapes by alternating between estimating point correspondences and alignment [8,9]. In our case we do not estimate correspondences or alignment explicitly and we do not rely on hand-engineered part templates or pairwise terms. We instead leverage graph attention to determine and weigh pairs of points on different shapes. We integrate these weights in our cross-shape convolution scheme to hierarchically learn point representations.

Developing such cross-shape convolution approach poses a number of technical challenges. First, performing graph convolution across all-pairs of points and all-pairs of shapes becomes prohibitively expensive for large input collections of shapes. Our architecture learns global shape descriptors along with a *pairwise shape compatibility* function that allows us to efficiently select a set of candidate shapes and assess their usefulness for cross-shape convolution for each input shape. For example, given an input office chair, it is more useful to allow interactions of its points with points of another office chair rather than a stool. Furthermore, given a point on a shape, its interactions with other points of another shape are not equally important. We incorporate a *cross-shape attention* function that predicts the degree of interaction between pairs of points on different shapes. Another challenge is that training the above attention function requires discovering shapes useful for cross-shape convolution in the first place. To this end, during training, we maintain a sparse graph (called “shape

collection graph”, Figure 1), whose nodes represent training shapes and edges specify which pairs of shapes should interact for cross-shape convolution. During training, the graph edges are dynamically updated according to the learned pairwise shape compatibility function such that increasingly more informative shapes are selected for cross-shape convolution per each training shape. At test time, the shape collection graph is augmented with additional nodes representing test shapes (Figure 1). New edges are added connecting them to training shapes for propagating representations from relevant training shapes through our learned cross-shape convolution.

Our architecture integrates the popular DGCNN network [1] as backbone. We extended it with our cross-shape convolution layers and trained our new architecture end-to-end for semantic shape segmentation. Our experiments indicate significantly higher performance on the recent PartNet dataset [10]. Compared to our backbone, we found an improvement of 3.3% in part IoU on average in PartNet for fine-grained shape segmentation. In particular, we found that **our method improves the part IoU by 6% on average for PartNet categories with limited number of training shapes (< 300)** compared to our backbone, demonstrating the utility of our cross-shape convolution scheme especially in such scenarios of limited training data.

2 Related work

We briefly overview related work on 3D deep learning for point clouds. We also discuss cross-attention networks developed in other domains.

3D deep learning for processing point clouds. Several different types of neural networks have been proposed for processing point sets over the recent years. After the pioneering work of PointNet [11,12], several works further investigated hierarchical point aggregation mechanisms to better model the spatial distribution of points [13,14,15]. Alternatively, point clouds can be projected onto local views [16,17,18,19] and processed as regular grids through image-based convolutional networks. Another line of work converts point representations into volumetric grids [20,21,22,23,24,25] and processes them through 3D convolutions. Instead of uniform grids, hierarchical space partitioning structures (e.g., kd-trees, lattices) can be used to define regular convolutions [26,27,28,29,30]. Another type of networks incorporate point-wise convolution operators to directly process point clouds [31,32,33,34,35,36,37,38,39,40,41,42]. Alternatively, shapes can be treated as graphs by connecting each point to other points within neighborhoods in a feature space. Then graph convolution and pooling operations can be performed either in the spatial domain [1,43,44,45,46,2,47,3,4,5,6,48,15], or spectral domain [49,50,51,52]. Attention mechanisms have also been investigated to modulate the importance of graph edges and point-wise convolutions [33,5,6,7]. Finally, graph neural network approaches have been shown to model non-local interactions between points within the same shape [1,3,5,48].

None of the above approaches have investigated the possibility of extending convolution or attention across shapes in a collection. Our work shows that

these cross-shape operations are not only possible, but also provide significant improvements over conventional approaches.

Cross-attention in other domains. Our method is inspired by recent cross-attention models proposed for video classification, image classification, keypoint recognition, and image-text matching. Wang et al. [53] introduced non-local networks that allow any image query position to perceive features of all the other positions within the same image or across frames in a video. To avoid huge attention maps, Huang et al. proposes a “criss-cross” attention module [54] to maintain sparse connections for each position in image feature maps. Cao et al. [55] simplifies non-local blocks with query-independent attention maps [55]. Lee et al. [56] propose cross-attention between text and images to discover latent alignments between images regions and words in a sentence. Hou et al. [57] models the semantic relevance between class and query feature maps in images through cross-attention to localize more relevant image regions for classification and generate more discriminative features. Finally, Sarlin et al. [58] learns keypoint matching between two indoor images from different viewpoints by leveraging self-attention and cross-attention to boost the receptive field of local descriptors and allow cross-image communication.

Our method introduces attention mechanisms across 3D shapes. Apart from the obvious need to develop cross-attention and non-local convolution operations on the irregular format of point clouds, our method also models the input training collection as a graph whose edges connect instances (shapes) deemed as useful for training our cross-attention and non-local convolution operations. The usefulness of shape pairs is determined based on a learned shape compatibility function trained together with the rest of our network.

3 Method

Overview. Given an input collection of 3D shapes represented as point clouds, the goal of our method is to propagate representations from one shape to another, and perform semantic segmentation. To perform this propagation, we propose cross-shape, non-local convolution operations. These operations update point representations on one shape by performing non-local convolutions with point representations originating from other shapes. This interaction is regulated by a *Cross-Shape Attention (CSA)* layer that predicts how much pairs of points on different shapes should influence each other. Since performing this exchange of information between all-pairs of shapes can become computationally expensive for large collections, we also present a technique to embed shapes of the input collection in a sparse graph, which we call *shape collection graph*. The nodes of this graph are shapes (Figure 1), and edges specify which pairs of shapes should interact. The edges in this graph also carry weights indicating the *compatibility* of two shapes for cross-convolution. During training time, this graph is dynamically constructed based on the input training shapes. At test time, the graph

is augmented with additional nodes representing test shapes, and edges represent connections between test and training shapes such that the information propagates from the training to the test set.

In the following Section 3.1, we first describe our cross-shape attention layer for a pair of shapes. We then discuss its generalization to multiple shapes along with the pairwise shape compatibility function in Section 3.2. We discuss our network architecture in 3.3, and its training along with the construction of the shape collection graph in Section 3.4. Finally, we discuss the augmentation of the collection graph at test time in Section 3.5.

3.1 Cross-shape attention for a pair of shapes

We now introduce our Cross-Shape Attention (CSA) layer for processing a pair of shapes. We assume that both shapes are represented as sets of points and that each point is equipped with a D -dimensional representation. Our layer is agnostic to the specifics of the point representation. It can be either raw input (e.g., 3D point positions) or learned representations extracted from existing point processing networks. In our implementation, we used point representations produced by the widely popular DGCNN [1]. Given a shape m with point representations stacked in a $P_m \times D$ matrix \mathbf{X}_m , and a shape n with point representations similarly stacked in a $P_n \times D$ matrix \mathbf{X}_n , (P_m, P_n are the number of points in the two shapes), the output of our layer are new point-wise representations for both shapes:

$$\mathbf{X}'_m = f(\mathbf{X}_m, \mathbf{X}_n; \mathbf{W}), \quad \mathbf{X}'_n = f(\mathbf{X}_n, \mathbf{X}_m; \mathbf{W}) \quad (1)$$

where f is our cross-shape attention function with learned parameters \mathbf{W} . The function implements the transformations explained in the next paragraphs.

Key and query intermediate representations. Inspired by recent attention networks [59], we first transform the input point representations of the first shape in the pair to intermediate representations, called “query” representations. The input point representations of the second shape are transformed to intermediate “key” representations. The keys will be compared to queries to determine the degree of influence of one point on another. Specifically, in the case of processing the shape pair (m, n) , these transformations are expressed as follows:

$$\mathbf{q}_{m,i} = \mathbf{W}_q \mathbf{x}_{m,i} \quad \text{and} \quad \mathbf{k}_{n,j} = \mathbf{W}_k \mathbf{x}_{n,j} \quad (2)$$

where $\mathbf{x}_{m,i}$ is the representation of point i on shape m , $\mathbf{x}_{n,j}$ is the representation of point j on shape n , \mathbf{W}_q and \mathbf{W}_k are $D \times D$ learned weight matrices. The same $\mathbf{W}_q, \mathbf{W}_k$ matrices are applied to all points i of the first shape and points j of the second shape respectively to ensure invariance to point permutations. Processing the reverse pair $(\mathbf{X}_n, \mathbf{X}_m)$ yields different key and query representations i.e., the layer is not invariant to the order of the two shapes in the pair. As a result, the influences of one point to another will be asymmetric, as explained below.



Fig. 2: Visualization of cross-shape attention matrices between shape pairs from the upper layers of our network. On the odd columns, we show each input shape with their query region \mathcal{R} marked as red. On the even columns, we visualize heatmaps on its paired shape to highlight the total attention the points receive from the query region using $\sum_{i \in \mathcal{R}} A_{m,n}[i, *]$. The point representations on the query regions of the shapes in the odd columns will be mostly affected by the redder regions of their paired shapes in the even columns. The visualization shows that points that lie on geometrically and semantically similar regions across shapes are more likely to interact in our cross-shape convolution. Interactions seem sparse. Sometimes high attention is assigned to points that do not seem to share similar geometric structure (last column). This might be due to the possibility that attention can also focus on relations between different parts to promote dissimilarities in their point representations.

Pairwise point attention. The similarity of key and query representations is determined through scaled dot product [59]. This provides a measure of how much one shape point influences the point on the other shape, or in other words, how much cross-shape convolution should attend to this pair. By concatenating all keys and queries into matrices \mathbf{Q}_m and \mathbf{K}_n we can compute cross-shape attention for the input pair as follows:

$$\mathbf{A}_{m,n} = \text{softmax}\left(\frac{\mathbf{Q}_m \mathbf{K}_n^T}{\sqrt{D}}\right) \quad (3)$$

where $\mathbf{A}_{m,n}$ is a $P_m \times P_n$ matrix. We note that *softmax* is applied per row. Processing the reverse pair yields a different $P_n \times P_m$ attention matrix $\mathbf{A}_{n,m}$. This is possible due to the fact that shapes can generally vary in part structure. Letting the attention mechanism to adjust rows and columns of the two matrices without imposing symmetry may better account for structural shape differences. We visualize cross-shape attention matrices for characteristic shape pairs in Figure 2. Since our network is trained for segmentation, the cross-shape attention seems to correlate input points from one shape to points of similar parts from the other shape, especially in the upper layers of our network. However, cross-shape attention might also focus on points between different parts to promote dissimilarities in their representations.

Complexity. The above operation is expensive since it involves $O(P_m \cdot P_n)$ computation to update the attention matrix. The computation can be accelerated by using range searches with space partitioning structures (e.g., kd-tree on dot products [60]) built on top of the key representations, and updating the matrix only for key representations nearest to the queries. A simpler approach we experimented with is to maintain a subset of points as keys (uniformly sub-sampled from the original shape) i.e., attention matrix becomes $P_m \times P'_n$, where P'_n is the number of sub-sampled keys (see also supplementary material for its effect). In this manner, the attention matrix becomes sparser.

Cross-shape convolution. We now define the non-local, cross-shape convolution operator that uses the above pairwise attention matrix to update the point representations for shape m :

$$\mathbf{x}'_{m,i} = \sum_{j=1}^{P_n} \mathbf{A}_{m,n}[i,j] \mathbf{W}_v \mathbf{x}_{n,j} \quad (4)$$

where \mathbf{W}_v is a learned $D \times D$ transformation (same for all points to ensure invariance to permutations), and $\mathbf{A}_{m,n}[i,j]$ accesses the corresponding point attention value (a scalar) for the pair (i,j) . To accelerate the computation, we can skip the summation for points j not associated with keys due to sub-sampling.

Self-shape attention. The pairwise point attention of Eq. 3 and non-local convolution operator of Eq. 4 can also be applied to a pair that consists of the shape and itself. In this case, our CSA layer implements a form of Self-Shape Attention (SSA), enabling long-range interactions between shape points modulated by our pairwise point attention mechanism.

3.2 Cross-shape attention for multiple shapes

We now generalize the non-local convolution of Eq. 4 to handle updates from multiple shapes, and also combine cross-shape attention with self-shape attention. Here we assume that the input to our CSA layer is a shape m from an input collection, and a set of other shapes $\mathcal{C}(m)$ deemed as compatible for cross-shape convolution with this shape. We discuss how this set is selected in Section 3.4 during training, and Section 3.5 during testing. Given a set of shapes as input, our CSA layer outputs point representations for shape m as follows:

$$\mathbf{x}'_{m,i} = \sum_{n \in \{\mathcal{C}(m), m\}} c(m,n) \sum_{j=1}^{P_n} \mathbf{A}_{m,n}[i,j] \mathbf{W}_v \mathbf{x}_{n,j} \quad (5)$$

where $c(m,n)$ is a learned pairwise function that outputs a single scalar representing the compatibility between shape m and n . The key idea of the above operation is to update point representations of shape m as a weighted average

of attention-modulated representations computed by using other shapes as well as the shape itself. The compatibility function $c(m, n)$ assesses these weights that different shapes should have for cross-shape convolution. It also implicitly provides the weight of self-shape attention when $m = n$.

Compatibility function. To compute the compatibility function, we first extract a global descriptor \mathbf{g}_m for the shape m and \mathbf{g}_n for each other shape n in the input compatible set $\mathcal{C}(m)$. These descriptors are extracted by a DGCNN network [1] dedicated to extract descriptors for shape compatibility. Specifically, it performs max and average pooling on individual point representations concatenated from all DGCNN point processing layers. Given point representations $\{\mathbf{y}_{m,i}\}$ for shape m , its global descriptor is computed as: $\mathbf{g}_m = [\max_i(\mathbf{y}_{m,i}); \text{mean}_i(\mathbf{y}_{m,i})]$, and similarly for the other shape descriptors. We then compare these global descriptors through scaled dot product attention [59]:

$$s(m, n) = (\mathbf{V}_q \mathbf{g}_m) \cdot (\mathbf{V}_k \mathbf{g}_n) / \sqrt{D'} \quad (6)$$

where \mathbf{V}_q , and \mathbf{V}_k are learned $D' \times D'$ transformations, and D' is the dimensionality of the global descriptors. The resulting comparison of descriptors provide us a measure of compatibility between two shapes (or a shape with itself). We normalize the above measures so that the sum of compatibilities of the shape m with all other shapes in the set $\mathcal{C}(m)$, including the self-compatibility (i.e., the weight of self-shape attention) is 1 through softmax:

$$c(m, n) = \frac{\exp(s(m, n))}{\sum_{n \in \{\mathcal{C}(m), m\}} \exp(s(m, n))} \quad (7)$$

As discussed in Section 3.4, our method learns the pairwise shape compatibilities to maximize the segmentation performance during training.

3.3 Architecture

We now discuss how we combined the CSA layers in our network architecture. We visualize our implemented architecture, called *CrossShapeNet*, in the case of processing a shape m along with another compatible shape n in Figure 3. As discussed earlier, we use DGCNN layers as our backbone. Specifically, given a shape with 3D point positions as input, DGCNN uses a sequence of graph convolution layers, called EdgeConv layers, to output per-point representations $\mathbf{X}_m^{(l)}$ for each EdgeConv layer l (and similarly for the other shape n). We attach a CSA layer processing the outputs of each corresponding EdgeConv layer. Each CSA layer has its own learned weight matrices $\mathbf{W}^{(l)}$ specific to each layer. It outputs new point-wise representations stacked in a matrix $\mathbf{X}_m'^{(l)}$ based on Equation 5.

Then all point representations from all CSA and corresponding DGCNN layers are concatenated for each point forming the final point-wise representations \mathbf{X}_m' . We observed that better performance can be achieved by applying CSA on all DGCNN layers of representations instead of only the last one. The point

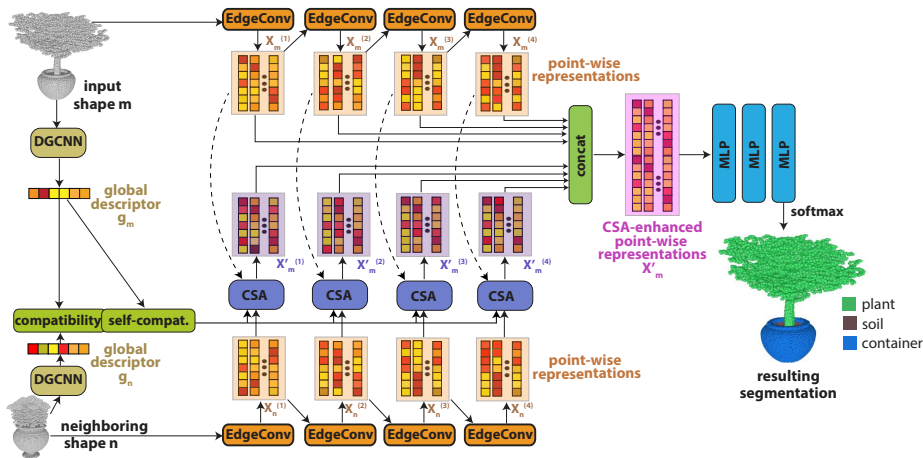


Fig. 3: Architecture of our network (*CrossShapeNet*). We demonstrate it for cross-shape convolution of the shape m on the top left with another shape n shown on the bottom left. The first stage of our architecture is to assess the compatibility of the shape pair, as well as the self-compatibility of the shape m with itself. Then a sequence of 4 *EdgeConv* layers [1] paired with our *Cross-Shape Attention (CSA)* layers process the input points and above compatibilities to produce new point representations for shape m , enhanced by interactions with other points from both shapes. The resulting segmentation is shown on the right.

representations \mathbf{X}'_m are mapped to part label probabilities through a three-layer MLP and softmax. We provide more detail about the exact configuration and dimension of layers in our supplementary material.

3.4 Training

We now discuss our training procedure to train *CrossShapeNet*. The input to our training procedure is a training collection of labeled point clouds with part annotations, along with a smaller annotated collection used for hold-out validation. To train our CSA layers, we first need to form compatible sets $C(m)$ for each shape m used in Equation 5. The compatible sets are created by defining the one-ring neighbors of each shape in the shape collection graph (Figure 1, left). We maintain one such graph for the training collection, and another graph for the hold-out validation one. Below we discuss the initialization of the collection graphs, then discuss training of *CrossShapeNet* and updates to the graphs.

Shape collection graph initialization. We first connect each shape to its K nearest neighbors computed through global descriptors extracted from DGCNN [1] pretrained for classification on ModelNet40. These neighbors form an initial estimate of our “compatible” shape set $C(m)$ for each training shape m . The $K = |C(m)|$ is an input parameter to our method. We discuss its effect for

different values in our results section. Given this initial collection graph, each training shape can be processed through *CrossShapeNet*. We train it using cross-entropy: $L_{ce} = \sum_{m,i} \log(\mathbf{P}_{m,i}[c])$ where c denotes the ground-truth label for point i of training shape m , and $\mathbf{P}_{m,i}$ the output probability distribution over part labels per point. During training, the compatibility function also receives supervisory signal from the above part labeling loss. As a result, the pairwise shape compatibilities, self-compatibilities, and global shape descriptors used for their computation, are updated during training.

We also create a collection graph in our hold-out validation set using the same procedure and monitor hold-out validation loss. We train *CrossShapeNet* until the validation loss saturates, then we update the shape collection graph.

Shape collection graph update. Based on the updated global shape descriptors, new K nearest neighbors for each shape are picked based on the compatibility measure of Equation 6. These new neighbors result in updating the collection graphs for training and hold-out validation, and in turn form new “compatible” sets of shapes for each training shape. After this update, we re-run training with the above loss for more epochs.

We alternate between shape collection graph updating and *CrossShapeNet* training. The hold-out validation collection graph is also updated and used to monitor training, and stop it when the validation performance saturates.

Implementation details. We use the Adam optimizer with 0.001 learning rate. The batch size depends on the the number of neighbors K : we use batch sizes 6, 3 and 2 for CrossShapeNet with $K=1, 3$ and 5 respectively. We provide more details on our architecture in the supplementary material. We note that our implementation will become publicly available after review process.

3.5 Test time

At test time, for each test shape, we find the nearest K training shapes to define its neighborhood in the shape collection graph based on our compatibility measure (Equation 6). Since the measure involves dot products between descriptors, the computation can run reasonably fast in our implementation (it can also be accelerated with kd-trees [60]). The trained *CrossShapeNet* is then used to extract the part annotations for the test shapes.

4 Results

We evaluated our method for fine-grained shape segmentation both qualitatively and quantitatively. Below we discuss the dataset, evaluation metrics, and comparisons with our backbone (DGCNN [1]) and other state-of-the-art models.

	bed	bott	chair	clock	dish	disp	door	ear	fauc	knife	lamp	micro	frid	stor	table	trash	vase	avg
DGCNN	33.1	47.5	36.4	22.2	45.7	78.7	23.1	40.6	52.3	28.3	20.0	34.9	28.5	41.2	27.0	43.1	50.7	38.4
CrossShapeNet-SSA	29.5	48.8	34.7	24.8	44.2	78.2	33.0	44.8	54.0	31.8	20.4	42.7	35.5	41.6	25.1	40.5	49.9	40.0
CrossShapeNet-K1	34.7	44.4	34.5	23.2	40.6	78.3	41.8	46.6	51.5	37.8	19.4	41.5	34.1	43.1	29.2	45.8	51.0	41.0
CrossShapeNet-K3	35.6	45.7	35.4	28.8	31.3	79.0	35.0	46.2	53.9	33.7	20.3	49.7	39.7	43.9	27.8	42.6	52.2	41.2
CrossShapeNet-K5	36.9	41.1	34.2	31.3	43.8	77.6	24.2	46.1	54.0	38.0	19.7	48.8	41.5	41.8	27.7	46.0	52.7	41.5
N shapes	212	464	6400	579	201	954	245	247	708	384	2271	212	207	2303	8309	340	1104	

Table 1: Part-category mIOU on PartNet. We report results for different variants of our method and our backbone. The last row shows the number of shapes per category for reference. The last column reports the average over all 17 categories. The shapes are split to training-validation-test sets with the ratio 70%:10%:20% in PartNet.

Dataset. We use the recent *PartNet* dataset [10] for training and evaluating our method according to its provided training, validation, and testing splits. Similarly to the evaluation done in [3] and [15], our evaluation focuses on the fine-grained level of semantic segmentation, which includes 17 out of the 24 object categories present in the PartNet dataset. To train our method, we used 2.5K points randomly sub-sampled from the original 10K points provided for each training shape in PartNet. This resolution is similar to the one used in the original DGCNN for shape classification and segmentation [1]. We performed this sub-sampling to enable faster training. Our network and also DGCNN, can handle different number of points as input. Thus, at test time, we process all 10K points for test shapes. Compared to testing on 2.5K points and then upsampling the network outputs to 10K points through nearest neighbor interpolation, our strategy of processing the higher resolution point clouds directly worked better (see supplementary material for more details). For evaluation, we use the standard performance metrics of part and shape mIoU to evaluate our method and alternatives. Like other methods ([3] and [15]), we emphasize part IoU in our evaluation, since it better reflects the labeling accuracy of fine-grained parts in each shape.

Comparison with our backbone. Our cross-shape convolution layers are built on top of the EdgeConv layers of DGCNN [1]. Thus, the primary goal in our evaluation is to examine *how much cross-shape convolution improves our backbone*.

We train our backbone in the same training splits under the same 2.5K point cloud resolution, using only points as input (no normals), and testing on 10K points as in our network. Training and testing of DGCNN and our network is done for each shape category separately.

Table 1 reports part IoU for the DGCNN backbone, and the following variants of *CrossShapeNet*: (a) *CrossShapeNet-SSA* uses CSA layers that compute attention and perform convolution of each shape with itself only i.e., using only self-shape attention based on Equation 4, (b) *CrossShapeNet-K1* is a network that uses the general form of CSA layers (Equation 5) combining self-shape attention and cross-shape attention of each shape with $K = 1$ other shape (c)

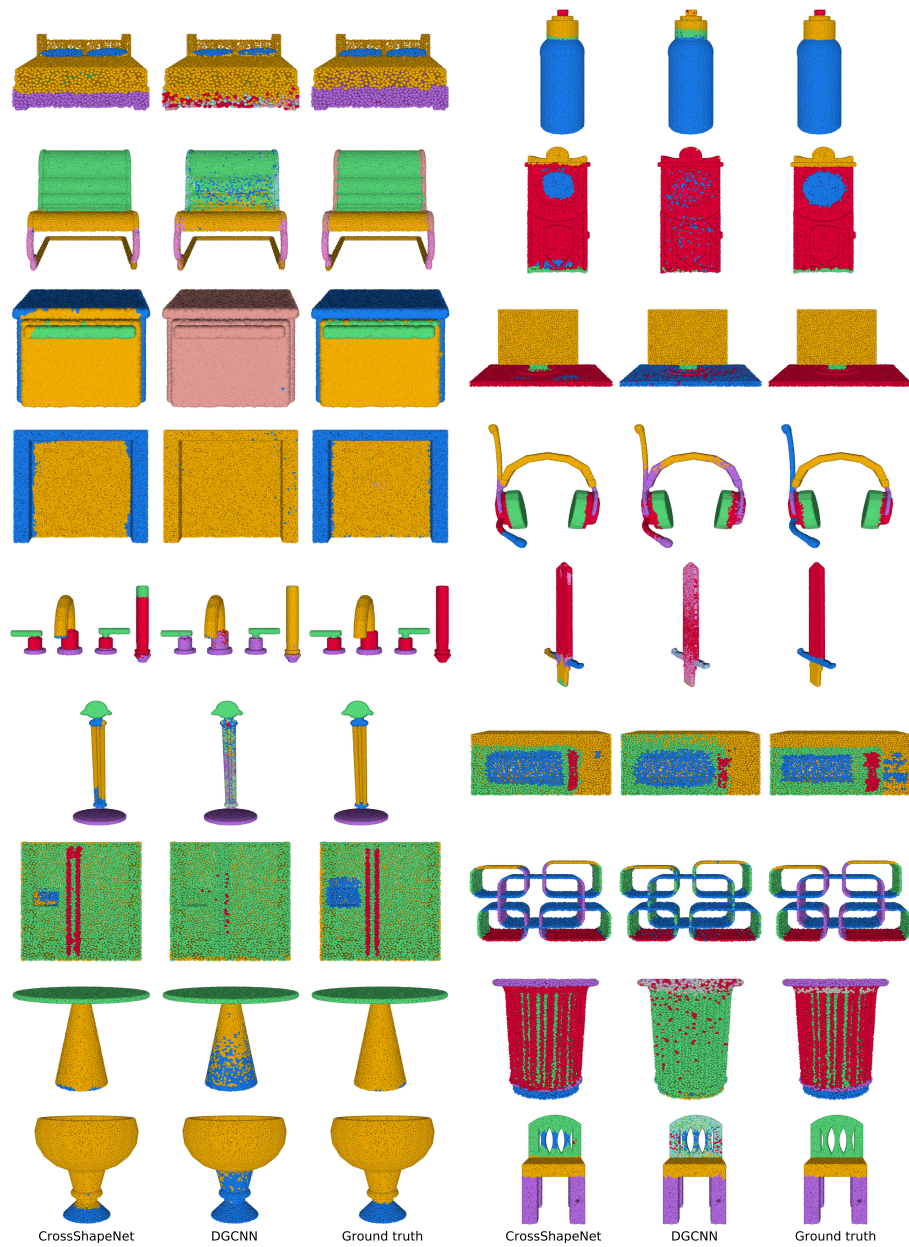


Fig. 4: **Qualitative comparison** between CrossShapeNet, our DGCNN backbone and ground truth. Different colors represent different semantic labels.

CrossShapeNet-K3 is same as above but using $K = 3$ other shapes in cross-shape convolution. (d) *CrossShapeNet-K5* is same as above but using $K = 5$ other shapes.

Based on the results, we make the following observations. First, the performance increases using self-shape attention in most classes relative to our backbone (average part mIoU increases from 38.4% \rightarrow 40.0%). Then performance is further increased in most classes using cross-shape convolution based on $K = 1$ (average part mIoU increases from 38.4% \rightarrow 41.0%). The best performance is achieved using $K = 5$ in most classes (average part mIoU increases from 38.4% \rightarrow 41.5%). In terms of shape IoU, our best cross-shape convolution model *CrossShapeNet-K5* also increases it (44.4% \rightarrow 50.1%, see supplementary material for more details.)

Our main observation is that the improvements are more common in categories with relatively fewer training shapes:

- For categories with less than 1000 training shapes (i.e., excluding Chair, Lamp, Storage Furniture, Table and Vase), the average part IoU increases from 39.8% in DGCNN to 44.1% in *CrossShapeNet-K5*, representing an increase of 4.3%.
- For categories with less than 300 training shapes (these are: Bed, Dish-washer, Door, Earphone, Microwave, Refrigerator), the average part mIoU raises from 34.2% in DGCNN to 40.2% in *CrossShapeNet-K5*, representing an increase of 6%.

Figure 4 shows characteristic examples of point cloud segmentations based on our DGCNN backbone and *CrossShapeNet-K5* along with ground-truth segmentations. We observe that our network is able to provide finer level of segmentation, especially for smaller parts or parts with complex geometry.

Comparisons with state-of-the-art. We now discuss comparisons with two other methods that recently demonstrated state-of-the-art performance in PartNet. ResGCN [3] showed the benefit of residual/dense connections and dilated convolutions in graph neural networks, making them also very deep. DeepConvPN [15] introduces multi-resolution, residual, and cross-link blocks to process multi-scale and multi-resolution information to improve the original PointNet++ [12] and DGCNN [1] modules, also doubling the number of their layers. Our work instead focused on the concept of cross-shape attention, which can be considered as orthogonal to the improvements of the two other models.

Table 2 shows part IoU for each of the 17 PartNet categories for which the other two methods report their performance. For these comparisons, we report the performance of “CrossShapeNet-K5” along with another variant, called “CrossShapeNet-K-Val”. For this variant, we train three cross-shape convolution models for $K = 1, 3, 5$ in each shape category, and selected the model whose K yielded the best hold-out validation performance (part IoU). In the last column, we report the part IoU averaged over the 17 categories.

Our “CrossShapeNet-K5” model compares favorably to the above two methods, resulting on an average part IoU which is 0.7% lower than DeepConvPN,

	bed	bott	chair	clock	dish	disp	door	ear	fauc	knife	lamp	micro	frid	stor	table	trash	vase	avg
CrossShapeNet-K5	36.9	41.1	34.2	31.3	43.8	77.6	24.2	46.1	54.0	38.0	19.7	48.8	41.5	41.8	27.7	46.0	52.7	41.5
CrossShapeNet-K-Val	36.9	44.4	35.3	31.3	43.8	79.0	41.8	46.2	51.5	38.0	20.3	49.7	39.7	43.9	29.2	45.8	52.7	42.9
ResGCN-28 [3]	35.2	36.8	33.8	32.6	52.7	84.4	42.5	41.9	49.7	35.4	20.0	54.3	46.1	42.5	14.8	49.7	50.8	42.5
DeepConvPN [15]	29.5	42.1	41.8	34.7	33.2	81.6	34.8	49.6	53.0	44.8	28.4	33.5	32.3	41.1	36.3	43.1	57.8	42.2
N shapes	212	464	6400	579	201	954	245	247	708	384	2271	212	207	2303	8309	340	1104	

Table 2: Comparison with state-of-the-art methods (part mIOU).

and 1% lower than the much deeper ResGCN-28 (28 layers). Selecting the best performing K value for cross-shape convolution (“CrossShapeNet-K-Val”) has a small edge of 0.4% better performance compared to the state-of-the-art. We emphasize that these comparisons are not necessarily fair since ResGCN and DeepConvPN are deeper, while CrossShapeNet-K-Val is based on an ensemble. The comparisons can be used as reference to evaluate the orthogonal improvements of all these models.

5 Conclusion

We presented a new type of graph neural network for 3D shape processing that enables point interactions and information exchange between shapes in an input collection. Our experiments demonstrated significant improvements of using our cross-shape convolution and attention layers over conventional graph convolution approaches, such as DGCNN [1], especially in the regime of limited number of training examples.

There are several avenues for future work. First, computing self- and cross-attention is intensive for large or even moderately-sized point clouds. In our preliminary experiments we investigated a subsampling approach to make the cross-shape attention matrix sparser, yet we believe that using hierarchical models and spatial subdivision structures would be better alternatives. Second, it would be interesting to incorporate deeper and wider backbones in our method, such as the ones proposed in [3] and [15]. In addition, we did not fully exploit the concept of the shape collection graph. It is possible to enable interactions also between test shapes. Finally, we suspect that our method will be useful for other tasks in point cloud processing, such as classification and correspondences, especially in few-shot learning regimes.

References

1. Wang, Y., Sun, Y., Liu, Z., Sarma, S.E., Bronstein, M.M., Solomon, J.M.: Dynamic graph cnn for learning on point clouds. *ACM Trans. Graph.* **38**(5) (2019)
2. Liu, Y., Fan, B., Xiang, S., Pan, C.: Relation-shape convolutional neural network for point cloud analysis. In: *IEEE Conference on Computer Vision and Pattern Recognition (CVPR)*. (2019) 8895–8904

3. Li, G., Muller, M., Thabet, A., Ghanem, B.: Deepgcns: Can gcns go as deep as cnns? In: IEEE International Conference on Computer Vision (CVPR). (2019) 9267–9276
4. Jiang, L., Zhao, H., Liu, S., Shen, X., Fu, C.W., Jia, J.: Hierarchical point-edge interaction network for point cloud semantic segmentation. In: IEEE International Conference on Computer Vision (CVPR). (2019) 10433–10441
5. Xu, Q., Sun, X., ying Wu, C., Wang, P., Neumann, U.: Grid-gcn for fast and scalable point cloud learning. arXiv preprint arXiv:1912.02984 (2019)
6. Wang, L., Huang, Y., Hou, Y., Zhang, S., Shan, J.: Graph attention convolution for point cloud semantic segmentation. In: IEEE Conference on Computer Vision and Pattern Recognition (CVPR). (2019) 10296–10305
7. Yunxiao, S., Haoyu, F., Jing, Z., Yi, F.: Pairwise attention encoding for point cloud feature learning. In: Proceedings of the International Conference on 3D Vision (3DV). (2019)
8. Kim, V.G., Li, W., Mitra, N.J., Chaudhuri, S., DiVerdi, S., Funkhouser, T.: Learning part-based templates from large collections of 3d shapes. *ACM Trans. Graph.* **32**(4) (2013)
9. Huang, H., Kalogerakis, E., Marlin, B.: Analysis and synthesis of 3d shape families via deep-learned generative models of surfaces. *Computer Graphics Forum* **34**(5) (2015)
10. Mo, K., Zhu, S., Chang, A.X., Yi, L., Tripathi, S., Guibas, L.J., Su, H.: Partnet: A large-scale benchmark for fine-grained and hierarchical part-level 3d object understanding. In: IEEE Conference on Computer Vision and Pattern Recognition (CVPR). (2019) 909–918
11. Qi, C.R., Su, H., Mo, K., Guibas, L.: Pointnet: Deep learning on point sets for 3d classification and segmentation. In: IEEE Conference on Computer Vision and Pattern Recognition (CVPR). (2017) 652–660
12. Qi, C.R., Yi, L., Su, H., Guibas, L.J.: Pointnet++: Deep hierarchical feature learning on point sets in a metric space. In: International Conference on Neural Information Processing Systems (NeurIPS). (2017)
13. Li, J., Chen, B., Lee, G.: So-net: Self-organizing network for point cloud analysis. In: Proceedings of the IEEE Conference on Computer Vision and Pattern Recognition (CVPR). (06 2018)
14. Srivastava, N., Goh, H., Salakhutdinov, R.: Geometric capsule autoencoders for 3d point clouds. arXiv preprint arXiv:1912.03310 (2019)
15. Le, E.T., Kokkinos, I., Mitra, N.J.: Going deeper with point networks. arXiv preprint arXiv:1907.00960 (2019)
16. Su, H., Maji, S., Kalogerakis, E., Learned-Miller, E.: Multi-view convolutional neural networks for 3d shape recognition. In: IEEE International Conference on Computer Vision (ICCV). (2015) 945–953
17. Qi, C.R., Su, H., Nießner, M., Dai, A., Yan, M., Guibas, L.J.: Volumetric and multi-view cnns for object classification on 3d data. In: IEEE Conference on Computer Vision and Pattern Recognition (CVPR). (2016) 5648–5656
18. Kalogerakis, E., Averkiou, M., Maji, S., Chaudhuri, S.: 3d shape segmentation with projective convolutional networks. In: IEEE Conference on Computer Vision and Pattern Recognition (CVPR). (2017) 3779–3788
19. Huang, H., Kalogerakis, E., Chaudhuri, S., Ceylan, D., Kim, V.G., Yumer, E.: Learning local shape descriptors from part correspondences with multiview convolutional networks. *ACM Transactions on Graphics* **37**(1) (2017)

20. Wu, Z., Song, S., Khosla, A., Yu, F., Zhang, L., Tang, X., Xiao, J.: 3d shapenets: A deep representation for volumetric shapes. In: IEEE Conference on Computer Vision and Pattern Recognition (CVPR). (2015) 1912–1920
21. Maturana, D., Scherer, S.: Voxnet: A 3d convolutional neural network for real-time object recognition. In: IEEE International Conference on Intelligent Robots and Systems (IROS), IEEE (2015) 922–928
22. Dai, A., Chang, A.X., Savva, M., Halber, M., Funkhouser, T., Nießner, M.: Scannet: Richly-annotated 3d reconstructions of indoor scenes. In: IEEE Conference on Computer Vision and Pattern Recognition (CVPR). (2017) 5828–5839
23. Rethage, D., Wald, J., Sturm, J., Navab, N., Tombari, F.: Fully-convolutional point networks for large-scale point clouds. In: European Conference on Computer Vision (ECCV). (2018) 596–611
24. Shi, S., Wang, X., Li, H.: Pointrcnn: 3d object proposal generation and detection from point cloud. In: IEEE Conference on Computer Vision and Pattern Recognition (CVPR). (June 2019) 770–779
25. Liu, Z., Tang, H., Lin, Y., Han, S.: Point-voxel cnn for efficient 3d deep learning. In: Advances in Neural Information Processing Systems (NeurIPS). (2019) 963–973
26. Riegler, G., Ulusoy, A.O., Geiger, A.: Octnet: Learning deep 3d representations at high resolutions. In: IEEE Conference on Computer Vision and Pattern Recognition (CVPR). (2017)
27. Klokov, R., Lempitsky, V.: Escape from cells: Deep KD-networks for the recognition of 3d point cloud models. In: IEEE International Conference on Computer Vision (CVPR). (2017) 863–872
28. Wang, P.S., Liu, Y., Guo, Y.X., Sun, C.Y., Tong, X.: O-CNN: Octree-based convolutional neural networks for 3D shape analysis. *ACM Transactions on Graphics* **36**(4) (2017)
29. Wang, P.S., Sun, C.Y., Liu, Y., Tong, X.: Adaptive O-CNN: A patch-based deep representation of 3d shapes. *ACM Trans. Graph.* **37**(6) (2018)
30. Su, H., Jampani, V., Sun, D., Maji, S., Kalogerakis, E., Yang, M.H., Kautz, J.: SPLATNet: Sparse lattice networks for point cloud processing. In: IEEE Conference on Computer Vision and Pattern Recognition (CVPR). (2018)
31. Li, Y., Bu, R., Sun, M., Wu, W., Di, X., Chen, B.: PointCNN: Convolution on x-transformed points. In: Advances in Neural Information Processing Systems (NeurIPS). (2018) 820–830
32. Hua, B.S., Tran, M.K., Yeung, S.K.: Pointwise convolutional neural networks. In: IEEE Conference on Computer Vision and Pattern Recognition (CVPR). (2018) 984–993
33. Xie, S., Liu, S., Chen, Z., Tu, Z.: Attentional shapecontextnet for point cloud recognition. In: IEEE Conference on Computer Vision and Pattern Recognition (CVPR). (2018) 4606–4615
34. Liu, Y., Fan, B., Meng, G., Lu, J., Xiang, S., Pan, C.: Densepoint: Learning densely contextual representation for efficient point cloud processing. In: IEEE International Conference on Computer Vision (ICCV). (2019) 5239–5248
35. Groh, F., Wieschollek, P., Lensch, H.P.A.: Flex-convolution (million-scale point-cloud learning beyond grid-worlds). In: Asian Conference on Computer Vision (ACCV). (2018)
36. Atzmon, M., Maron, H., Lipman, Y.: Point convolutional neural networks by extension operators. *ACM Trans. Graph.* **37**(4) (2018)
37. Hermosilla, P., Ritschel, T., Vázquez, P.P., Vinacua, A., Ropinski, T.: Monte carlo convolution for learning on non-uniformly sampled point clouds. *ACM Trans. Graph.* **37**(6) (2018)

38. Wang, S., Suo, S., Ma, W.C., Pokrovsky, A., Urtasun, R.: Deep parametric continuous convolutional neural networks. In: IEEE Conference on Computer Vision and Pattern Recognition (CVPR). (2018) 2589–2597
39. Xu, Y., Fan, T., Xu, M., Zeng, L., Qiao, Y.: Spidercnn: Deep learning on point sets with parameterized convolutional filters. arXiv preprint arXiv:1803.11527 (2018)
40. Wu, W., Qi, Z., Fuxin, L.: Pointconv: Deep convolutional networks on 3d point clouds. In: IEEE Conference on Computer Vision and Pattern Recognition (CVPR). (2019) 9621–9630
41. Komarichev, A., Zhong, Z., Hua, J.: A-CNN: Annularly convolutional neural networks on point clouds. In: IEEE Conference on Computer Vision and Pattern Recognition (CVPR). (2019) 7421–7430
42. Thomas, H., Qi, C.R., Deschaud, J.E., Marcotegui, B., Goulette, F., Guibas, L.J.: KPConv: Flexible and deformable convolution for point clouds. In: IEEE International Conference on Computer Vision (CVPR). (2019) 6411–6420
43. Shen, Y., Feng, C., Yang, Y., Tian, D.: Mining point cloud local structures by kernel correlation and graph pooling. In: IEEE Conference on Computer Vision and Pattern Recognition (CVPR). (2018) 4548–4557
44. Lan, S., Yu, R., Yu, G., Davis, L.S.: Modeling local geometric structure of 3d point clouds using geo-cnn. In: IEEE Conference on Computer Vision and Pattern Recognition (CVPR). (2019) 998–1008
45. Wang, C., Samari, B., Siddiqi, K.: Local spectral graph convolution for point set feature learning. arXiv preprint arXiv:1803.05827 (2018)
46. Zhang, K., Hao, M., Wang, J., de Silva, C.W., Fu, C.: Linked Dynamic Graph CNN: Learning on point cloud via linking hierarchical features. arXiv preprint arXiv:1904.10014 (2019)
47. Landrieu, L., Boussaha, M.: Point cloud oversegmentation with graph-structured deep metric learning. In: IEEE Conference on Computer Vision and Pattern Recognition (CVPR). (2019) 7440–7449
48. Han, W., Wen, C., Wang, C., Li, X., Li, Q.: Point2Node: Correlation learning of dynamic-node for point cloud feature modeling. arXiv preprint arXiv:1912.10775 (2019)
49. Yi, L., Su, H., Guo, X., Guibas, L.J.: SyncSpecCNN: Synchronized spectral cnn for 3d shape segmentation. In: IEEE Conference on Computer Vision and Pattern Recognition (CVPR). (2017) 2282–2290
50. Boscaini, D., Masci, J., Melzi, S., Bronstein, M.M., Castellani, U., Vandergheynst, P.: Learning class-specific descriptors for deformable shapes using localized spectral convolutional networks. In: Computer Graphics Forum. Volume 34., Wiley Online Library (2015) 13–23
51. Boscaini, D., Masci, J., Rodolà, E., Bronstein, M.: Learning shape correspondence with anisotropic convolutional neural networks. In: Advances in Neural Information Processing Systems (NeurIPS). (2016) 3189–3197
52. Monti, F., Boscaini, D., Masci, J., Rodola, E., Svoboda, J., Bronstein, M.M.: Geometric deep learning on graphs and manifolds using mixture model cnns. In: IEEE Conference on Computer Vision and Pattern Recognition (CVPR). (2017) 5115–5124
53. Wang, X., Girshick, R., Gupta, A., He, K.: Non-local neural networks. In: IEEE Conference on Computer Vision and Pattern Recognition (CVPR). (2018) 7794–7803
54. Huang, Z., Wang, X., Huang, L., Huang, C., Wei, Y., Liu, W.: CCNet: Criss-cross attention for semantic segmentation. In: IEEE International Conference on Computer Vision (CVPR). (2019) 603–612

55. Cao, Y., Xu, J., Lin, S., Wei, F., Hu, H.: GCNet: Non-local networks meet squeeze-excitation networks and beyond. In: IEEE International Conference on Computer Vision (CVPR) Workshops. (2019)
56. Lee, K.H., Chen, X., Hua, G., Hu, H., He, X.: Stacked cross attention for image-text matching. (2018) 201–216
57. Hou, R., Chang, H., Bingpeng, M., Shan, S., Chen, X.: Cross attention network for few-shot classification. In: Advances in Neural Information Processing Systems (NeurIPS). (2019) 4005–4016
58. Sarlin, P.E., DeTone, D., Malisiewicz, T., Rabinovich, A.: Superglue: Learning feature matching with graph neural networks. arXiv preprint arXiv:1911.11763 (2019)
59. Vaswani, A., Shazeer, N., Parmar, N., Uszkoreit, J., Jones, L., Gomez, A.N., Kaiser, L., Polosukhin, I.: Attention is all you need. In: Advances in Neural Information Processing Systems (NeurIPS). (2017) 5998–6008
60. Ram, P., Gray, A.G.: Maximum inner-product search using tree data-structures. arXiv preprint arXiv:1202.6101 (2012)
61. Wu, Y., He, K.: Group normalization. In: European Conference on Computer Vision (ECCV). (2018) 3–19
62. Kingma, D.P., Ba, J.: Adam: A method for stochastic optimization. arXiv preprint arXiv:1412.6980 (2014)

A Supplementary experiments

In this appendix, we provide additional experiments and comparisons regarding: (a) sub-sampling vs keeping the original keys for CSA, (b) upsampling point labels versus testing directly on higher resolution point clouds. We also report evaluation based on the shape mIoU metric. Finally, we provide additional architecture and training details, as well as plots demonstrating the utility of updating the shape collection graph during training.

Sub-sampling keys. As explained in Section 3.1, to accelerate the cross-convolution operator, the number of keys can be reduced to sparsify the cross-shape attention matrix. We conducted an experiment to evaluate the effect of this sub-sampling. Specifically, we reduced the keys down to 1K points by random sub-sampling (a 2.5x factor in reduction for this experiment). This led to a faster forward pass through all four CSA layers by factor of 1.5x. Specifically, a feed-forward pass of 2 shapes in a CSA layer took 5.0 ms instead of 7.5 ms on a NVidia RTX 2070 used for benchmarking. Results are presented in Table 3 in terms of part IoU (“CrossShapeNetSub-K3” means CSA with sub-sampling). They suggest that downsampling keys during training is computationally beneficial, while it does not lead to performance drop. As discussed in our main paper, investigating other strategies, such as a hierarchical approach or using kd-trees in high-dimensional spaces, could prove more beneficial.

Upsampling point labels versus testing on higher-resolution directly. As discussed in our results section, we trained all variants of architecture and our backbone DGCNN on 2.5K points, then tested on the 10K points provided in the PartNet benchmark.

One possibility to deal with this different resolution is to simply make predictions on 2.5K points (i.e., at lower resolution), then perform a *nearest-neighbor upsampling* to transfer the labels to 10K points (i.e., each point in the higher-resolution shape copies the label from the nearest point in the low-resolution representation).

Another possibility is to pass the original, higher-resolution test points directly to our architecture (and backbone). However, to perform this direct processing of higher-resolution of point clouds, we need to perform an *adjustment of the receptive field of our backbone* (DGCNN). During training, our backbone uses

	bed	bott	chair	clock	dish	disp	door	ear	fauc	knife	lamp	micro	frid	stor	table	trash	vase	avg
CrossShapeNetSub-K3	37.9	44.9	34.4	32.4	36.5	78.8	37.0	43.6	51.8	35.1	19.3	45.9	38.8	43.4	25.7	45.6	52.3	41.4
CrossShapeNet-K3	35.6	45.7	35.4	28.8	31.3	79.0	35.0	46.2	53.9	33.7	20.3	49.7	39.7	43.9	27.8	42.6	52.2	41.2
N shapes	212	464	6400	579	201	954	245	247	708	384	2271	212	207	2303	8309	340	1104	

Table 3: Part mIOU on PartNet for cross-shape attention model with subsampled vs original keys (CrossShapeNetSub-K3 vs CrossShapeNet-K3 respectively). The last row shows the number of shapes per category for reference.

$K = 20$ nearest neighbors in its EdgeConv layers. At test time, to achieve a similar receptive field in the higher-resolution point cloud, we increase $K = 20 \rightarrow 80$ at test time (since using the original number of neighbors would result in a smaller receptive field in the higher-resolution point cloud).

Table 4 shows a comparison of these two strategies: the nearest neighbor upsampling (“CrossShapeNet-K3-NN”) versus testing directly on the higher-resolution point cloud with receptive field adjustment (“CrossShapeNet-K3”). Since the nearest neighbor upsampling depends on the initial choice of the 2.5K sub-sampled subset and therefore has inherent randomness, we report results averaged over 5 test runs (where we randomly choose sub-sampled subsets each time for testing). Testing directly on the higher-resolution point cloud with the above receptive field adjustment yields better results. Its average part mIOU is higher by $\sim 1.3\%$ than using nearest neighbor upsampling.

We observed the same trend while testing our backbone alone i.e., DGCNN with nearest neighbor upsampling vs DGCNN processing higher-resolution point cloud at test time with the same receptive field adjustment.

	bed	bott	chair	clock	dish	disp	door	ear	fauc	knife	lamp	micro	frid	stor	table	trash	vase	avg
CrossShapeNet-K3-NN	32.7	43.2	36.5	28.0	30.4	78.4	34.7	43.9	52.3	32.2	20.6	44.7	38.2	39.6	29.4	42.5	51.0	39.9
CrossShapeNet-K3	35.6	45.7	35.4	28.8	31.3	79.0	35.0	46.2	53.9	33.7	20.3	49.7	39.7	43.9	27.8	42.6	52.2	41.2
N shapes	212	464	6400	579	201	954	245	247	708	384	2271	212	207	2303	8309	340	1104	

Table 4: Part mIOU on PartNet of the nearest neighbor upsampling strategy (“CrossShapeNet-K3-NN”) vs testing directly on the higher-resolution point cloud with receptive field adjustment (“CrossShapeNet-K3”).

B Evaluation wrt Shape mIoU

As discussed in our results section, we emphasized the use of part IoU in our evaluation similarly to prior work, since it better reflects the labeling accuracy of fine-grained parts in each shape.

For completeness, Table 5 reports the alternative shape mIoU metric. The results show that our method significantly improves the shape mIOU of our baseline model on average ($44.4\% \rightarrow 50.1\%$), and in the majority of classes.

C Implementation and training details.

Table 6 presents the layers of our “CrossShapeNet-K1” variant in detail (the “CrossShapeNet-K3” and “CrossShapeNet-K5” variants follow the same structure). The network takes a pair of *query* and *key* shapes as inputs. For the *query* shape, it outputs the probability of each part label per point. Layers 2-5 perform

	bed	bott	chair	clock	dish	disp	door	ear	fauc	knife	lamp	micro	frid	stor	table	trash	vase	avg
DGCNN	22.2	57.3	38.2	35.4	46.4	77.9	36.5	49.6	54.3	28.4	26.7	44.6	42.3	42.2	34.6	44.5	74.4	44.4
CrossShapeNet-K1	28.6	56.7	43.4	41.5	46.2	79.9	39.0	56.2	58.6	36.8	35.8	52.2	52.2	47.7	42.8	54.5	76.6	49.9
CrossShapeNet-K3	28.3	58.8	44.5	42.0	46.2	79.9	45.8	56.1	59.2	29.1	35.0	51.8	55.1	49.4	41.1	52.5	77.0	50.1
CrossShapeNet-K5	27.6	60.4	43.1	40.2	45.7	78.7	38.5	55.3	58.1	39.9	32.3	53.2	58.5	50.1	38.6	54.1	77.6	50.1
CrossShapeNet-BestVal	28.6	60.4	44.5	40.2	46.2	79.9	45.8	56.1	58.6	39.9	35.8	53.2	52.2	50.1	42.8	54.5	76.6	50.9
N shapes	212	464	6400	579	201	954	245	247	708	384	2271	212	207	2303	8309	340	1104	

Table 5: Shape mIoU on PartNet dataset. We report results on 10K points for all models. The last column reports the average over all 17 categories. The shapes are split to training-validation-test sets with the ratio 70%:10%:20% in PartNet.

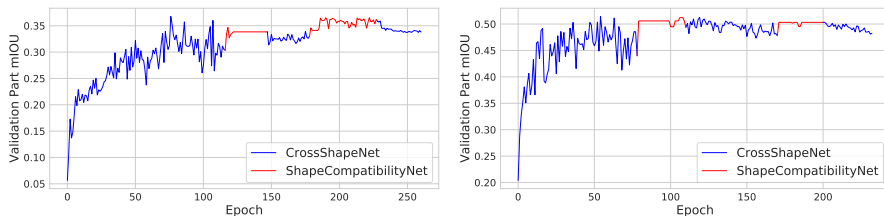


Fig. 5: Per-epoch evolution of part mIoU for CrossShapeNet-K5 on the validation splits of Clock (left) and Vase (right) categories over a couple of training iterations; during each iteration, we alternate (a) between CrossShapeNet training phase (in blue color), and (b) shape compatibility updating phase (in red color). We note that during the last phase of CrossShapeNet training, the performance slightly drops due to overfitting. At this point, we stop training. Yet, the shape compatibility updates slightly raised the performance before that.

EdgeConv on *query* and *key* shapes separately; layer 6 creates the DGCNN representation of the shapes; Layers 7-10 compute Cross-Shape Attention (CSA) for each EdgeConv layer; layers 12-15 compute Self-Shape Attention (SSA); layer 17 computes the similarity between *query* and *key* points (see Table 7); layer 18 computes similarity between *query* and *query* points (Table 7); layer 19 takes softmax over outputs of layers 17-18; layer 20 takes weighted sum of cross-shape attention and self-shape attention based on these values; layer 21 concatenates DGCNN and Cross/Self-Shape Attention representations; layers 22-27 perform MLP on constructed representations to produce part label probabilities. For CrossShapeNet we use group normalization [61] in EdgeConv layers since our batch sizes are very small (6 for K1, 3 for K3, 2 for K5).

Table 7 shows the architecture of the sub-module used to determine the compatibility between two shapes (see Section 3.2, “compatibility function paragraph”). We call this sub-module as “ShapeCompatibilityNet” architecture. The network takes the *query* and *key* shapes as inputs and outputs the compatibility between them which is used to weigh the Cross- and Self-Shape Attention. Layers 2-5 perform EdgeConv on *query* and *key* shapes separately; layer 6 creates DGCNN representation of shapes; Layer 7 performs a linear transformation of the previous layer; layers 8-10 perform max and average poolings over points

Index	Layer	out
1	Input _{query} , Input _{key}	$N \times 3$
2	EdgeConv(out(1), 3, 64) + GN	$N \times 64$
3	EdgeConv(out(2), 64, 64) + GN	$N \times 64$
4	EdgeConv(out(3), 64, 128) + GN	$N \times 128$
5	EdgeConv(out(3), 128, 256) + GN	$N \times 256$
6	CAT(out(2), out(3), out(4), out(5))	$N \times 512$
7	CSA(out(1) _{query} , out(1) _{key})	$N \times 64$
8	CSA(out(2) _{query} , out(2) _{key})	$N \times 64$
9	CSA(out(3) _{query} , out(3) _{key})	$N \times 128$
10	CSA(out(4) _{query} , out(4) _{key})	$N \times 256$
11	CAT(out(7), out(8), out(9), out(10))	$N \times 512$
12	SSA(out(1) _{query} , out(1) _{key})	$N \times 64$
13	SSA(out(2) _{query} , out(2) _{key})	$N \times 64$
14	SSA(out(3) _{query} , out(3) _{key})	$N \times 128$
15	SSA(out(4) _{query} , out(4) _{key})	$N \times 256$
16	CAT(out(12), out(13), out(14), out(15))	$N \times 512$
17	SIM(Input _{query} , Input _{key})	1×1
18	SIM(Input _{query} , Input _{query})	1×1
19	SIM-CSA, SIM-SSA = Softmax(out(17), out(18))	2×1
20	SIM-CSA*out(11) + SIM-SSA*out(16)	$N \times 512$
21	CAT(out(6), out(20))	$N \times 1024$
22	FC(out(21), 1024) + ReLU	$N \times 1024$
23	FC(out(22), 512) + ReLU + Dropout(0.5)	$N \times 512$
24	FC(out(23), 256) + ReLU + Dropout(0.5)	$N \times 256$
25	FC(out(24), 128) + ReLU + Dropout(0.5)	$N \times 128$
26	FC(out(25), $N_{classes}$)	$N \times N_{classes}$
27	SemanticLabel =Softmax(out(25))	$N \times N_{classes}$

Table 6: **Architecture of the CrossShapeNet-K1.** EdgeConv: edge convolution, CSA: Cross-Shape Attention, SA: Self-Shape Attention, SIM: ShapeCompatibilityNet (see Table 7), GN: group normalization, RELU: rectified linear unit, FC: fully connected layer, CAT: concatenate tensors along the second dimension

and concatenate them to compute global shape descriptors; layers 11-12 perform queries/keys transformations of the global descriptors; layer 13 computes similarity as scaled dot product between the *query* and *key* descriptors.

We initialize the weights for the ShapeCompatibilityNet from a model pre-trained on ModelNet40 dataset [20]. We do not replace the batch normalization with group normalization here since we use a pretrained network. For additional information on our DGCNN backbone, we refer the reader to [1].

Training details Here we describe the training procedure for CrossShapeNet in more detail. For optimization we use the Adam optimizer [62] with learning rate 0.001 and $(\beta_1, \beta_2) = (0.9, 0.999)$. We initialize our training procedure by training

Index	Layer	out
1	Input _{query} , Input _{key}	$N \times 3$
2	EdgeConv(out(1), 3, 64)	$N \times 64$
3	EdgeConv(out(2), 64, 128)	$N \times 128$
4	EdgeConv(out(3), 128, 128)	$N \times 128$
5	EdgeConv(out(3), 128, 256)	$N \times 256$
6	CAT(out(2), out(3), out(4), out(5))	$N \times 512$
7	CONV1D(out(6), 1024)	$N \times 1024$
8	AMP(out(7))	1×1024
9	AAP(out(7))	1×1024
10	CAT(out(8), out(9))	1×2048
11	REP _{query} = FC _{query} (out(10) _{query} , 2048)	1×2048
12	REP _{key} = FC _{key} (out(10) _{key} , 2048)	1×2048
13	SIM(query, key) = REP _{query} · REP _{key} / $\sqrt{2048}$	1×1

Table 7: **Architecture of the ShapeCompatibilityNet.** EdgeConv: edge convolution, FC: fully connected layer, CAT: concatenate tensors along the second dimension, AMP: adaptive max-pooling along the first dimension, AAP: adaptive average-pooling along the first dimension.

CrossShapeNet using a pretrained ShapeCompatibility sub-module (pretrained on ModelNet40 for classification). We keep the ShapeCompatibility parameters frozen, while training the rest of the network. Then, once validation accuracy saturates, we load the best current model from our checkpoint and switch to training the ShapeCompatibility sub-module, again until we observe saturation in the validation accuracy. We then update the collection shape graph (i.e., the compatible neighbors per shape). We keep training by alternating between these two phases: (a) training the CrossShapeNet layers (while keeping the rest frozen), (b) the ShapeCompatibility layers and updating the collection shape graph. Overall, we perform five such alternating training iterations: three for CrossShapeNet and two for ShapeCompatibilityNet. Figure 5 shows the evolution of the part IoU in the validation set for Clock (left) and Vases (right) in the case of “CrossShapeNet-K5” during the training epochs for the above phases. There is an improvement in performance when the ShapeCompatibility network and collection graph is updated.